Supplement of Atmos. Chem. Phys., 20, 805–827, 2020
https://doi.org/10.5194/acp-20-805-2020-supplement

Atmospheric Chemistry and Physics
Open Access
EGU

Supplement of

Investigation of the global methane budget over 1980–2017 using GFDL-AM4.1

Jian He et al.

Correspondence to: Jian He (jian.he@noaa.gov)

S1. Observational data

Table S1. List of NOAA-GMD marine boundary layer (MBL) sites

Code	Name	State	Country	Latitude	Longitude	Elevation (m)
ALT	Alert	Nunavut	Canada	82.451	-62.507	190
AMS	Amsterdam Island	N/A	France	-37.798	77.538	55
ASC	Ascension Island	N/A	United Kingdom	-7.967	-14.4	85
AVI	St. Croix	Virgin Islands	United States	17.75	-64.75	3
BME	St. Davids Head	Bermuda	United Kingdom	32.368	-64.648	12
BMW	Tudor Hill	Bermuda	United Kingdom	32.265	-64.879	30
BRW	Barrow	Alaska	United States	71.323	-156.611	11
CBA	Cold Bay	Alaska	United States	55.21	-162.72	21.3
CGO	Cape Grim	Tasmania	Australia	-40.683	144.69	94
CHR	Christmas Island	N/A	Republic of Kiribati	1.7	-157.152	0
CMO	Cape Meares	Oregon	United States	45.478	-123.969	30
CRZ	Crozet Island	N/A	France	-46.434	51.848	197
EIC	Easter Island	N/A	Chile	-27.16	-109.428	47
GMI	Mariana Islands	N/A	Guam	13.386	144.656	0
HBA	Halley Station	Antarctica	United Kingdom	-75.605	-26.21	30
ICE	Storhofdi	Vestmannaeyjar	Iceland	63.4	-20.288	118
KEY	Key Biscayne	Florida	United States	25.665	-80.158	1
KUM	Cape Kumukahi	Hawaii	United States	19.52	-154.82	3
MBC	Mould Bay	Northwest Territories	Canada	76.247	-119.353	30
MHD	Mace Head	County Galway	Ireland	53.326	-9.899	5
MID	Sand Island	Midway	United States	28.21	-177.38	11
POC000*	Pacific Ocean (0 N)	N/A	N/A	0	-155	10
POCN05*	Pacific Ocean (5 N)	N/A	N/A	5	-151	10
POCN10*	Pacific Ocean (10 N)	N/A	N/A	10	-149	10
POCN15*	Pacific Ocean (15 N)	N/A	N/A	15	-145	10
POCN20*	Pacific Ocean (20 N)	N/A	N/A	20	-141	10
POCN25*	Pacific Ocean (25 N)	N/A	N/A	25	-139	10
POCN30*	Pacific Ocean (30 N)	N/A	N/A	30	-135	10
POCS05*	Pacific Ocean (5 S)	N/A	N/A	-5	-159	10

POCS10*	Pacific Ocean (10 S)	N/A	N/A	-10	-161	10
POCS15*	Pacific Ocean (15 S)	N/A	N/A	-15	-164	10
POCS20*	Pacific Ocean (20 S)	N/A	N/A	-20	-167	10
POCS25*	Pacific Ocean (25 S)	N/A	N/A	-25	-171	10
POCS30*	Pacific Ocean (30 S)	N/A	N/A	-30	-176	10
POCS35*	Pacific Ocean (35 S)	N/A	N/A	-35	180	10
PSA	Palmer Station	Antarctica	United States	-64.92	-64	10
RPB	Ragged Point	N/A	Barbados	13.165	-59.432	15
SHM	Shemya Island	Alaska	United States	52.711	174.126	23
SMO	Tutuila	N/A	American Samoa	-14.247	-170.564	42
SPO	South Pole	Antarctica	United States	-89.98	-24.8	2810
STM	Ocean Station M	N/A	Norway	66	2	0
SYO	Syowa Station	Antarctica	Japan	-69.013	39.59	14
USH	Ushuaia	N/A	Argentina	-54.848	-68.311	12
ZEP	Ny-Alesund	Svalbard	Norway and Sweden	78.907	11.888	474

* Latitude values given for the POCN and POCS sites are the centers of latitude bands of +/- 2.5 degrees, and observations can fall anywhere within those bands.

Table S2. List of NOAA-GMD sites with at least 20-year observations

Code	Name	State	Country	Latitude	Longitude	Elevation (meters)
ALT	Alert	Nunavut	Canada	82.451	-62.507	190
ASC	Ascension Island	N/A	United Kingdom	-7.967	-14.4	85
ASK	Assekrem	N/A	Algeria	23.262	5.632	2710
AZR	Terceira Island	Azores	Portugal	38.766	-27.375	19
BMW	Tudor Hill	Bermuda	United Kingdom	32.265	-64.879	30
BRW	Barrow	Alaska	United States	71.323	-156.611	11
CBA	Cold Bay	Alaska	United States	55.21	-162.72	21.3
CGO	Cape Grim	Tasmania	Australia	-40.683	144.69	94
CHR	Christmas Island	N/A	Republic of Kiribati	1.7	-157.152	0
CRZ	Crozet Island	N/A	France	-46.434	51.848	197
EIC	Easter Island	N/A	Chile	-27.16	-109.428	47
GMI	Mariana Islands	N/A	Guam	13.386	144.656	0
HBA	Halley Station	Antarctica	United Kingdom	-75.605	-26.21	30
HUN	Hegyhatsal	N/A	Hungary	46.95	16.65	248
ICE	Storhofdi	Vestmannaeyjar	Iceland	63.4	-20.288	118
IZO	Izana	Tenerife	Spain	28.309	-16.499	2372.9
KEY	Key Biscayne	Florida	United States	25.665	-80.158	1
KUM	Cape Kumukahi	Hawaii	United States	19.52	-154.82	3
LEF	Park Falls	Wisconsin	United States	45.945	-90.273	472
MHD	Mace Head	County Galway	Ireland	53.326	-9.899	5
MID	Sand Island	Midway	United States	28.21	-177.38	11
MLO	Mauna Loa	Hawaii	United States	19.536	-155.576	3397
NWR	Niwot Ridge	Colorado	United States	40.053	-105.586	3523
POCN00*	Pacific Ocean (0 N)	N/A	N/A	0	-155	10
POCN05*	Pacific Ocean (5 N)	N/A	N/A	5	-151	10
POCN10*	Pacific Ocean (10 N)	N/A	N/A	10	-149	10
POCN15*	Pacific Ocean (15 N)	N/A	N/A	15	-145	10
POCN20*	Pacific Ocean (20 N)	N/A	N/A	20	-141	10
POCN25*	Pacific Ocean (25 N)	N/A	N/A	25	-139	10
POCN30*	Pacific Ocean (30 N)	N/A	N/A	30	-135	10

POCS05*	Pacific Ocean (5 S)	N/A	N/A	-5	-159	10
POCS10*	Pacific Ocean (10 S)	N/A	N/A	-10	-161	10
POCS15*	Pacific Ocean (15 S)	N/A	N/A	-15	-164	10
POCS20*	Pacific Ocean (20 S)	N/A	N/A	-20	-167	10
POCS25*	Pacific Ocean (25 S)	N/A	N/A	-25	-171	10
POCS30*	Pacific Ocean (30 S)	N/A	N/A	-30	-176	10
PSA	Palmer Station	Antarctica	United States	-64.92	-64	10
RPB	Ragged Point	N/A	Barbados	13.165	-59.432	15
SEY	Mahe Island	N/A	Seychelles	-4.682	55.532	2
SHM	Shemya Island	Alaska	United States	52.711	174.126	23
SMO	Tutuila	N/A	American Samoa	-14.247	-170.564	42
SPO	South Pole	Antarctica	United States	-89.98	-24.8	2810
STM	Ocean Station M	N/A	Norway	66	2	0
SYO	Syowa Station	Antarctica	Japan	-69.013	39.59	14
TAP	Tae-ahn Peninsula	N/A	Republic of Korea	36.738	126.133	16
USH	Ushuaia	N/A	Argentina	-54.848	-68.311	12
UTA	Wendover	Utah	United States	39.902	-113.718	1327
UUM	Ulaan Uul	N/A	Mongolia	44.452	111.096	1007
WIS	Weizmann Institute of Science at the Arava Institute	Ketura	Israel	29.965	35.06	151
WLG	Mt. Waliguan	N/A	Peoples Republic of China	36.288	100.896	3810
ZEP	Ny-Alesund	Svalbard	Norway and Sweden	78.907	11.888	474

* Latitude values given for the POCN and POCS sites are the centers of latitude bands of +/- 2.5 degrees, and observations can fall anywhere within those bands.

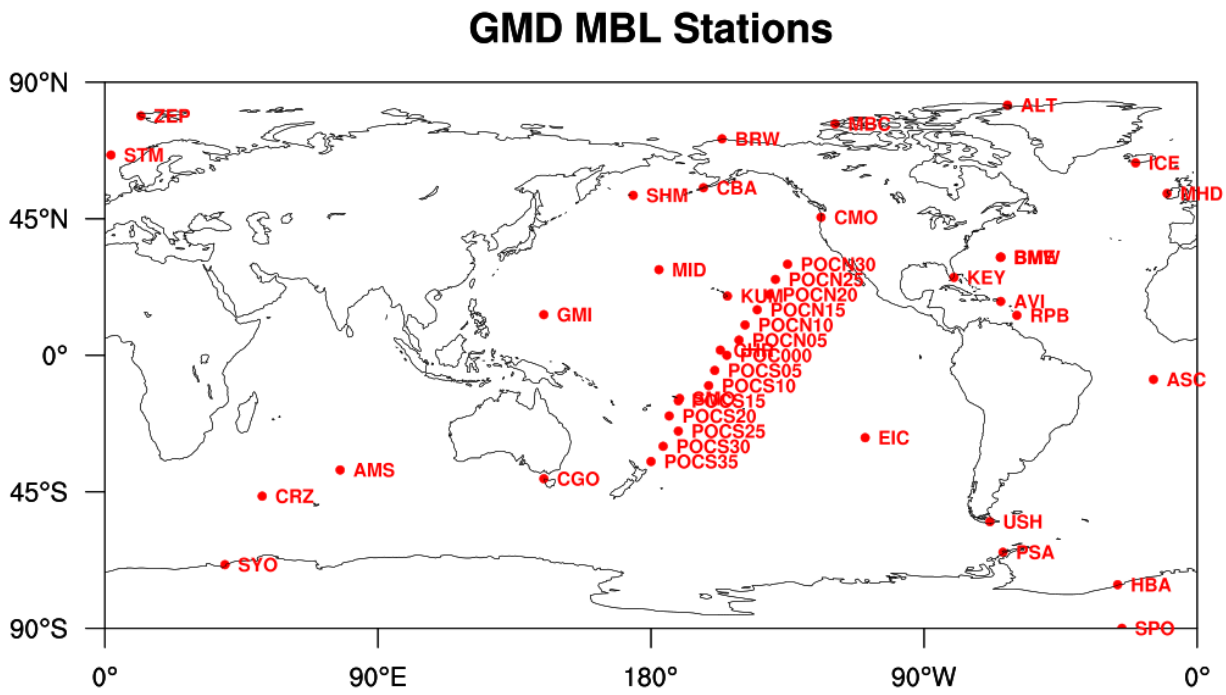

Figure S1. NOAA-GMD marine boundary layer (MBL) sites selected for background methane calculation.

S2. Evaluation of model simulations with initial emission inventories

We conducted two model simulations with the initial methane emissions inventories for 1980-2017: 1) the initial emissions described in Section 2.1 in the main text (referred to as "S0Orig"); 2) same as S0Orig but with time-varying wetland emissions based on an extended ensemble version of WetCHARTs for 2001-2015 (Bloom et al., 2017), which is referred to as "S0Origtswet". The model evaluation of the two simulations are shown in Figure S2 and S3.

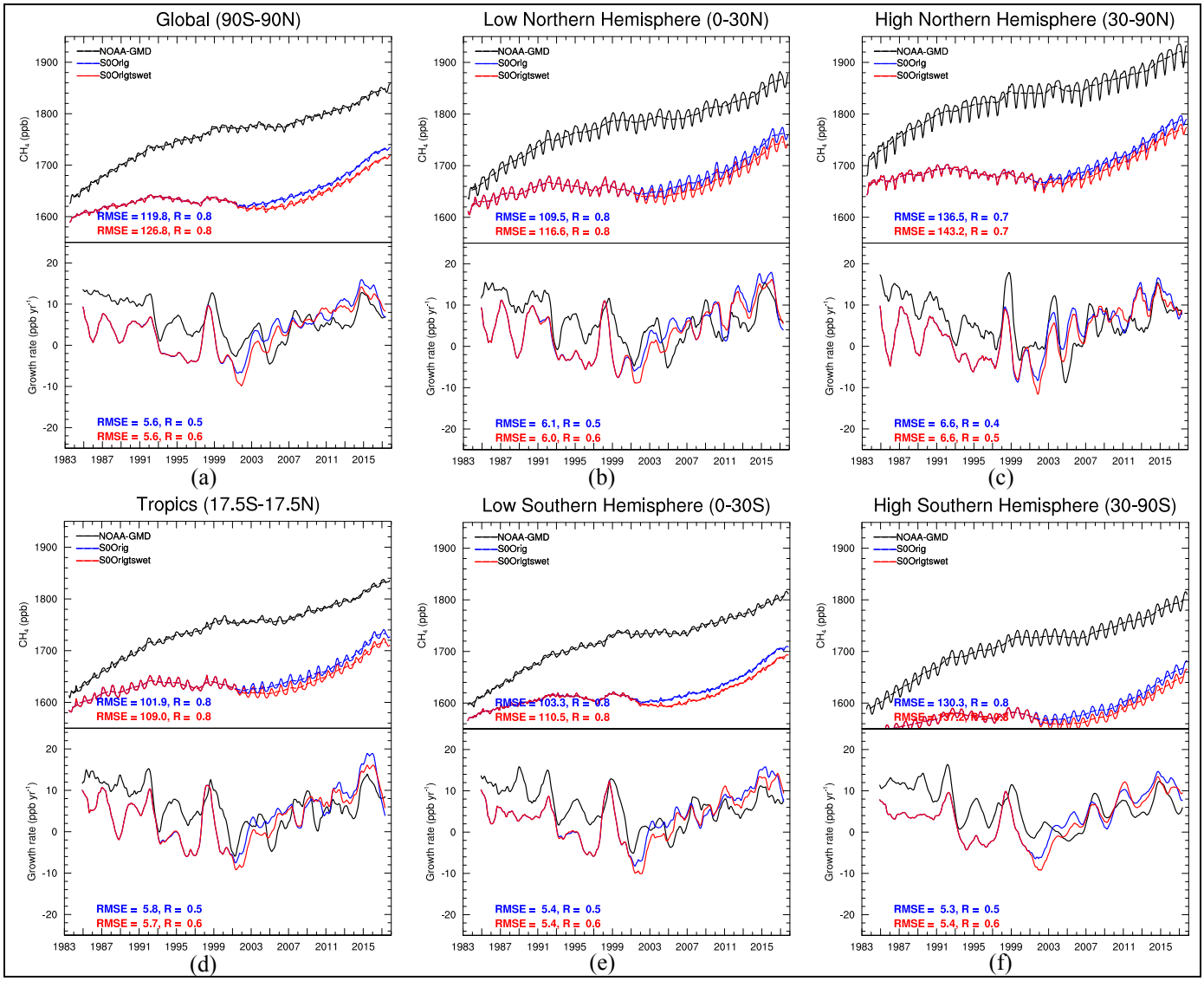

Figure S2. Comparison of GFDL-AM4.1 simulated methane concentrations and growth rates with NOAA-GMD surface observations with initial emission inventories. For the upper plot in each panel, dash line represents smoothed trends (i.e., 12-month running mean) from deseasonalized monthly data. A meridional curve (Tans et al., 1989) was fitted through NOAA-GMD site observations to get the latitudinal distribution of methane. A function fit consisting of yearly harmonics and a polynomial trend, with fast fourier transform and low pass filtering of the residuals are applied to the monthly mean methane DMF (Thoning et al., 1989; Thoning, 2019) to approximate the long-term trend. For the lower plot in each panel, the growth rates are calculated from the time derivative of the dash line in the corresponding upper plot.

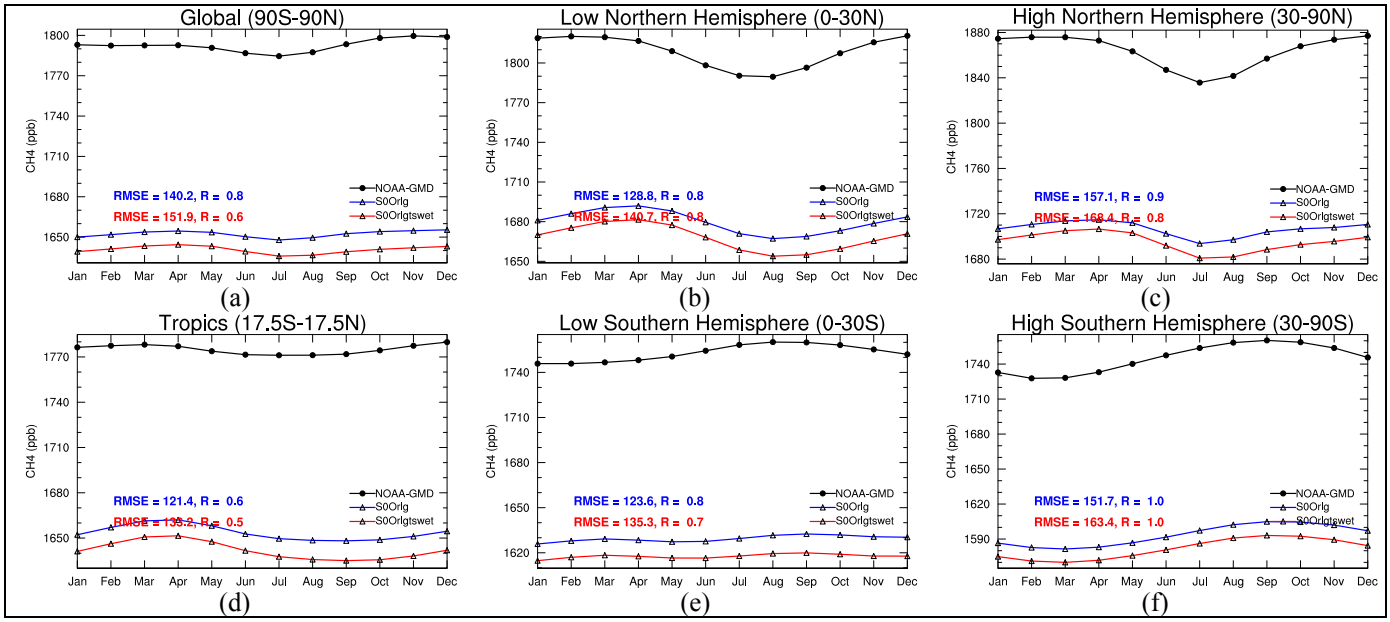

Figure S3. Comparison of GFDL-AM4.1 simulated methane seasonal cycles of 2001-2015 with NOAA-GMD surface observations with initial emission inventories.

S3. Surface evaluation at individual sites

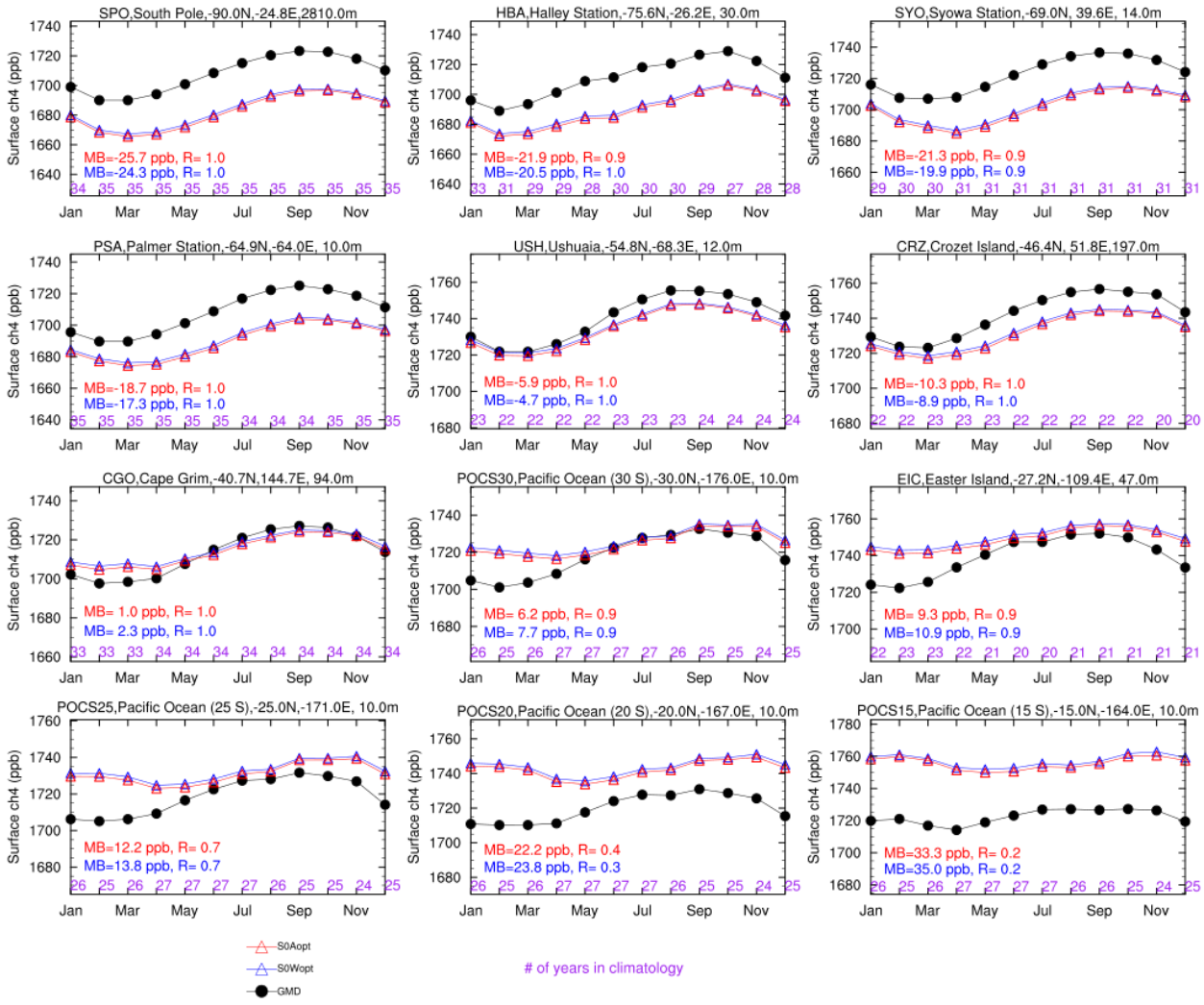

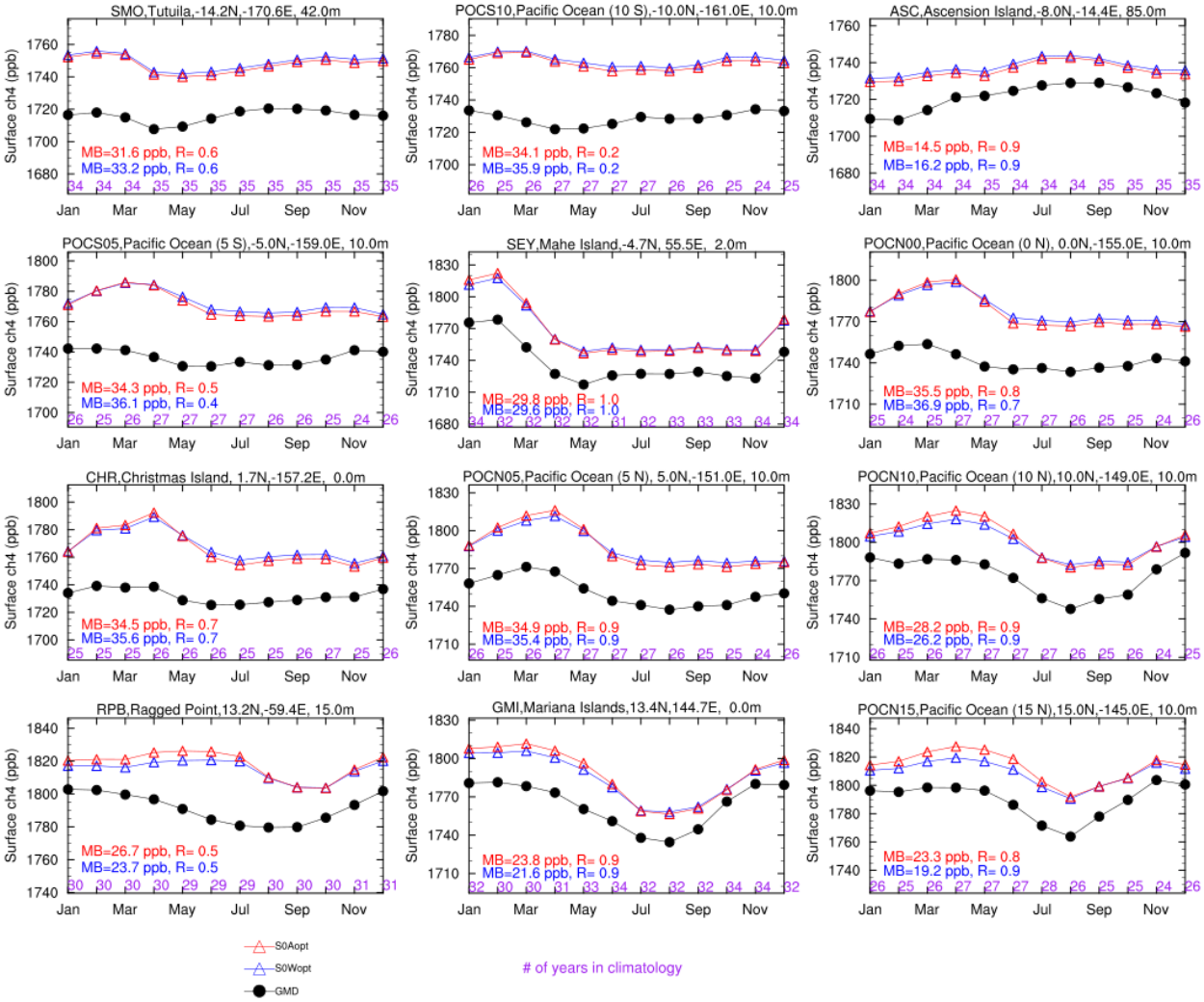
SMO,Tutuila,-14.2N,-170.6E, 42.0m
MB=31.6 ppb, R= 0.6
MB=33.2 ppb, R= 0.6
POCS10,Pacific Ocean (10 S),-10.0N,-161.0E, 10.0m
MB=34.1 ppb, R= 0.2
MB=35.9 ppb, R= 0.2
ASC,Ascension Island,-8.0N,-14.4E, 85.0m
MB=14.5 ppb, R= 0.9
MB=16.2 ppb, R= 0.9
POCS05,Pacific Ocean (5 S),-5.0N,-159.0E, 10.0m
MB=34.3 ppb, R= 0.5
MB=36.1 ppb, R= 0.4
SEY,Mahe Island,-4.7N, 55.5E, 2.0m
MB=29.8 ppb, R= 1.0
MB=29.6 ppb, R= 1.0
POCN00,Pacific Ocean (0 N), 0.0N,-155.0E, 10.0m
MB=35.5 ppb, R= 0.8
MB=36.9 ppb, R= 0.7
CHR,Christmas Island, 1.7N,-157.2E, 0.0m
MB=34.5 ppb, R= 0.7
MB=35.6 ppb, R= 0.7
POCN05,Pacific Ocean (5 N), 5.0N,-151.0E, 10.0m
MB=34.9 ppb, R= 0.9
MB=35.4 ppb, R= 0.9
POCN10,Pacific Ocean (10 N),10.0N,-149.0E, 10.0m
MB=28.2 ppb, R= 0.9
MB=26.2 ppb, R= 0.9
RPB,Ragged Point,13.2N,-59.4E, 15.0m
MB=26.7 ppb, R= 0.5
MB=23.7 ppb, R= 0.5
GMI,Mariana Islands,13.4N,144.7E, 0.0m
MB=23.8 ppb, R= 0.9
MB=21.6 ppb, R= 0.9
POCN15,Pacific Ocean (15 N),15.0N,-145.0E, 10.0m
MB=23.3 ppb, R= 0.8
MB=19.2 ppb, R= 0.9
Surface ch4 (ppb)
Jan Mar May Jul Sep Nov
S0Aopt
S0Wopt
GMD
# of years in climatology

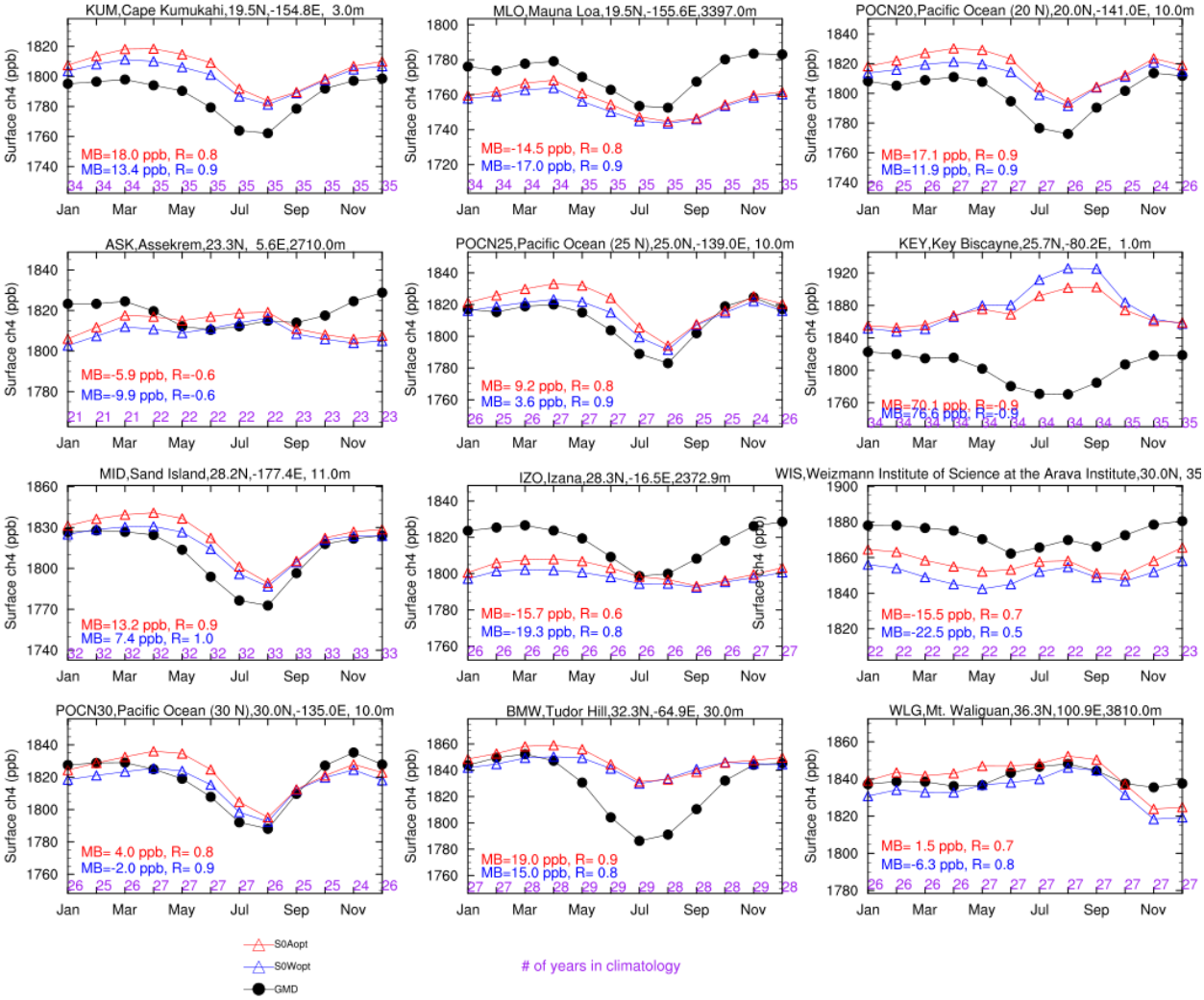
KUM,Cape Kumukahi,19.5N,-154.8E, 3.0m
MB=18.0 ppb, R= 0.8
MB=13.4 ppb, R= 0.9
MLO,Mauna Loa,19.5N,-155.6E,3397.0m
MB=-14.5 ppb, R= 0.8
MB=-17.0 ppb, R= 0.9
POCN20,Pacific Ocean (20 N),20.0N,-141.0E, 10.0m
MB=17.1 ppb, R= 0.9
MB=11.9 ppb, R= 0.9
ASK,Assekrem,23.3N, 5.6E,2710.0m
MB=-5.9 ppb, R=-0.6
MB=-9.9 ppb, R=-0.6
POCN25,Pacific Ocean (25 N),25.0N,-139.0E, 10.0m
MB= 9.2 ppb, R= 0.8
MB= 3.6 ppb, R= 0.9
KEY,Key Biscayne,25.7N,-80.2E, 1.0m
MB=70.1 ppb, R=-0.9
MB=76.6 ppb, R=-0.9
MID,Sand Island,28.2N,-177.4E, 11.0m
MB=13.2 ppb, R= 0.9
MB= 7.4 ppb, R= 1.0
IZO,Izana,28.3N,-16.5E,2372.9m
MB=-15.7 ppb, R= 0.6
MB=-19.3 ppb, R= 0.8
WIS,Weizmann Institute of Science at the Arava Institute,30.0N, 35
MB=-15.5 ppb, R= 0.7
MB=-22.5 ppb, R= 0.5
POCN30,Pacific Ocean (30 N),30.0N,-135.0E, 10.0m
MB= 4.0 ppb, R= 0.8
MB=-2.0 ppb, R= 0.9
BMW,Tudor Hill,32.3N,-64.9E, 30.0m
MB=19.0 ppb, R= 0.9
MB=15.0 ppb, R= 0.8
WLG,Mt. Waliguan,36.3N,100.9E,3810.0m
MB= 1.5 ppb, R= 0.7
MB=-6.3 ppb, R= 0.8
Surface ch4 (ppb)
Jan Mar May Jul Sep Nov
S0Aopt
S0Wopt
GMD
# of years in climatology

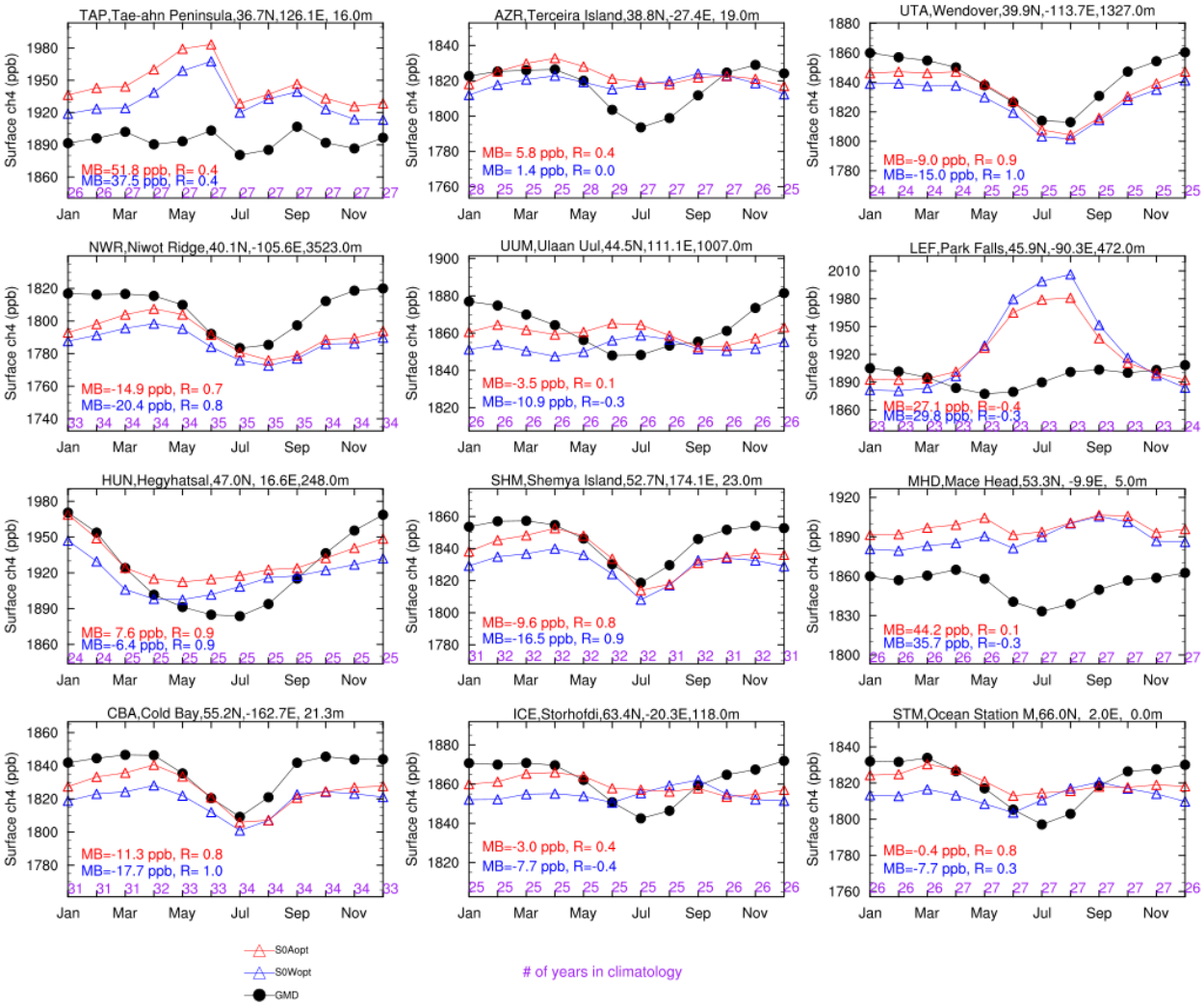
TAP,Tae-ahn Peninsula,36.7N,126.1E, 16.0m
MB=51.8 ppb, R= 0.4
MB=37.5 ppb, R= 0.4
AZR,Terceira Island,38.8N,-27.4E, 19.0m
MB= 5.8 ppb, R= 0.4
MB= 1.4 ppb, R= 0.0
UTA,Wendover,39.9N,-113.7E,1327.0m
MB=-9.0 ppb, R= 0.9
MB=-15.0 ppb, R= 1.0
NWR,Niwot Ridge,40.1N,-105.6E,3523.0m
MB=-14.9 ppb, R= 0.7
MB=-20.4 ppb, R= 0.8
UUM,Ulaan Uul,44.5N,111.1E,1007.0m
MB=-3.5 ppb, R= 0.1
MB=-10.9 ppb, R=-0.3
LEF,Park Falls,45.9N,-90.3E,472.0m
MB=27.1 ppb, R=-0.4
MB=29.8 ppb, R=-0.3
HUN,Hegyhatsal,47.0N, 16.6E,248.0m
MB= 7.6 ppb, R= 0.9
MB=-6.4 ppb, R= 0.9
SHM,Shemya Island,52.7N,174.1E, 23.0m
MB=-9.6 ppb, R= 0.8
MB=-16.5 ppb, R= 0.9
MHD,Mace Head,53.3N, -9.9E, 5.0m
MB=44.2 ppb, R= 0.1
MB=35.7 ppb, R=-0.3
CBA,Cold Bay,55.2N,-162.7E, 21.3m
MB=-11.3 ppb, R= 0.8
MB=-17.7 ppb, R= 1.0
ICE,Storhofdi,63.4N,-20.3E,118.0m
MB=-3.0 ppb, R= 0.4
MB=-7.7 ppb, R=-0.4
STM,Ocean Station M,66.0N, 2.0E, 0.0m
MB=-0.4 ppb, R= 0.8
MB=-7.7 ppb, R= 0.3
Surface ch4 (ppb)
Jan Mar May Jul Sep Nov
S0Aopt
S0Wopt
GMD
# of years in climatology

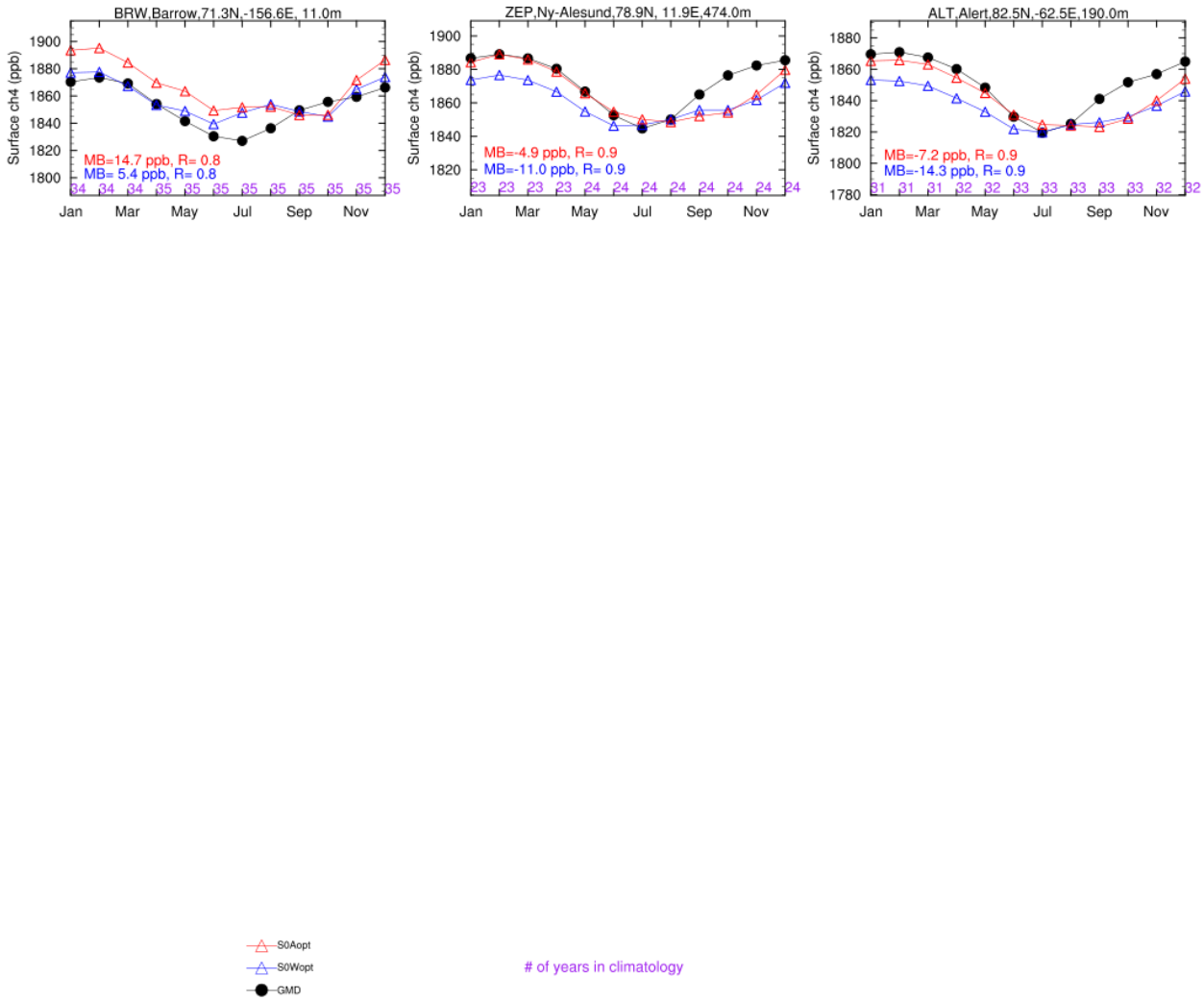

Figure S4. Comparisons of methane seasonal cycles against NOAA-GMD observations.

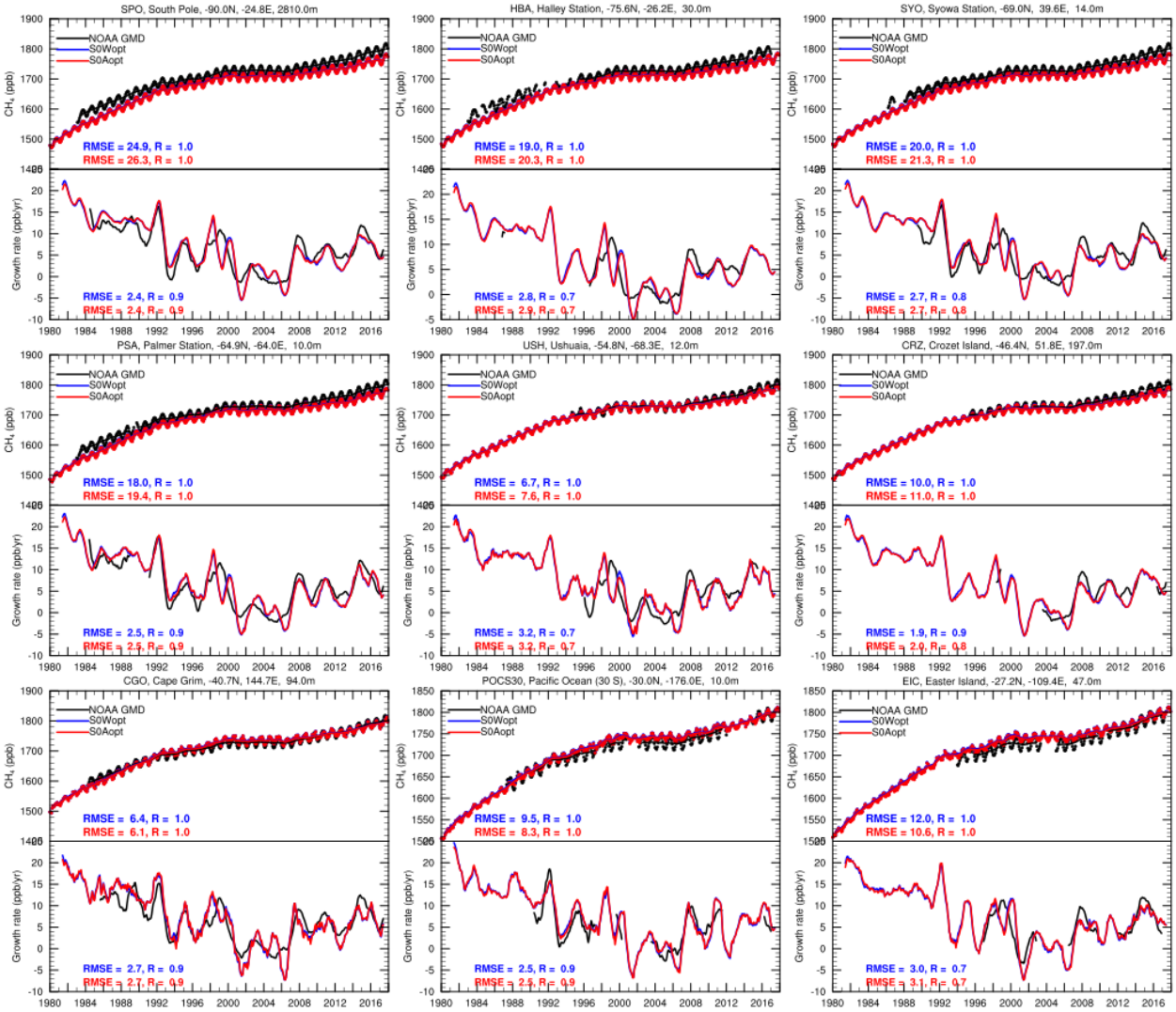
SPO, South Pole, -90.0N, -24.8E, 2810.0m
HBA, Halley Station, -75.6N, -26.2E, 30.0m
SYO, Syowa Station, -69.0N, 39.6E, 14.0m
PSA, Palmer Station, -64.9N, -64.0E, 10.0m
USH, Ushuaia, -54.8N, -68.3E, 12.0m
CRZ, Crozet Island, -46.4N, 51.8E, 197.0m
CGO, Cape Grim, -40.7N, 144.7E, 94.0m
POCS30, Pacific Ocean (30 S), -30.0N, -176.0E, 10.0m
EIC, Easter Island, -27.2N, -109.4E, 47.0m
NOAA GMD
S0Wopt
S0Aopt
CH4 (ppb)
Growth rate (ppb/yr)
RMSE = 24.9, R = 1.0
RMSE = 26.3, R = 1.0
RMSE = 2.4, R = 0.9
RMSE = 2.4, R = 0.9
RMSE = 19.0, R = 1.0
RMSE = 20.3, R = 1.0
RMSE = 2.8, R = 0.7
RMSE = 2.9, R = 0.7
RMSE = 20.0, R = 1.0
RMSE = 21.3, R = 1.0
RMSE = 2.7, R = 0.8
RMSE = 2.7, R = 0.8
RMSE = 18.0, R = 1.0
RMSE = 19.4, R = 1.0
RMSE = 2.5, R = 0.9
RMSE = 2.5, R = 0.9
RMSE = 6.7, R = 1.0
RMSE = 7.6, R = 1.0
RMSE = 3.2, R = 0.7
RMSE = 3.2, R = 0.7
RMSE = 10.0, R = 1.0
RMSE = 11.0, R = 1.0
RMSE = 1.9, R = 0.9
RMSE = 2.0, R = 0.8
RMSE = 6.4, R = 1.0
RMSE = 6.1, R = 1.0
RMSE = 2.7, R = 0.9
RMSE = 2.7, R = 0.9
RMSE = 9.5, R = 1.0
RMSE = 8.3, R = 1.0
RMSE = 2.5, R = 0.9
RMSE = 2.5, R = 0.9
RMSE = 12.0, R = 1.0
RMSE = 10.6, R = 1.0
RMSE = 3.0, R = 0.7
RMSE = 3.1, R = 0.7

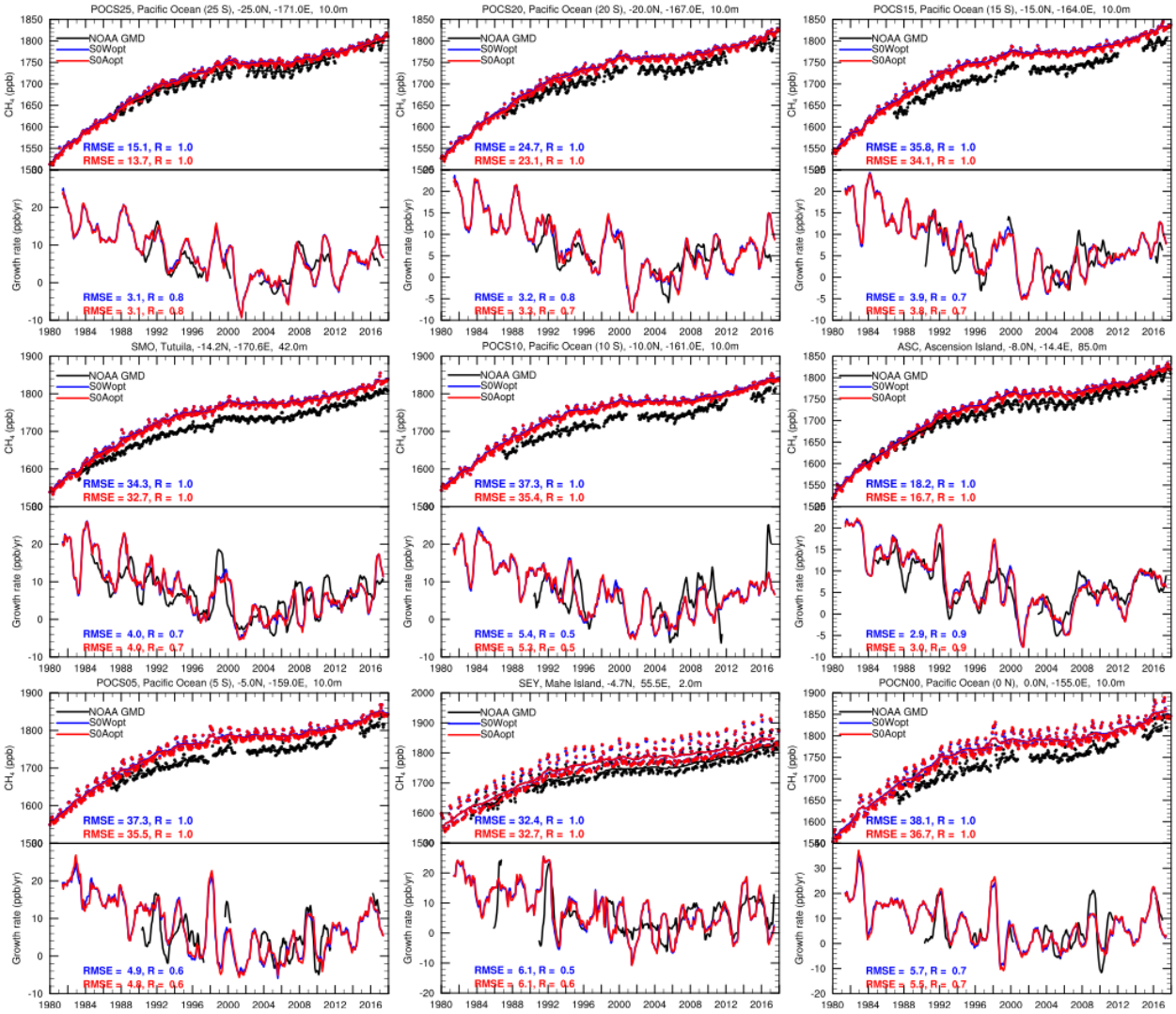
POCS25, Pacific Ocean (25 S), -25.0N, -171.0E, 10.0m
NOAA GMD
S0Wopt
S0Aopt
RMSE = 15.1, R = 1.0
RMSE = 13.7, R = 1.0
RMSE = 3.1, R = 0.8
RMSE = 3.1, R = 0.8
POCS20, Pacific Ocean (20 S), -20.0N, -167.0E, 10.0m
RMSE = 24.7, R = 1.0
RMSE = 23.1, R = 1.0
RMSE = 3.2, R = 0.8
RMSE = 3.2, R = 0.7
POCS15, Pacific Ocean (15 S), -15.0N, -164.0E, 10.0m
RMSE = 35.8, R = 1.0
RMSE = 34.1, R = 1.0
RMSE = 3.9, R = 0.7
RMSE = 3.9, R = 0.7
SMO, Tutuila, -14.2N, -170.6E, 42.0m
RMSE = 34.3, R = 1.0
RMSE = 32.7, R = 1.0
RMSE = 4.0, R = 0.7
RMSE = 4.0, R = 0.7
POCS10, Pacific Ocean (10 S), -10.0N, -161.0E, 10.0m
RMSE = 37.3, R = 1.0
RMSE = 35.4, R = 1.0
RMSE = 5.4, R = 0.5
RMSE = 5.2, R = 0.5
ASC, Ascension Island, -8.0N, -14.4E, 85.0m
RMSE = 18.2, R = 1.0
RMSE = 16.7, R = 1.0
RMSE = 2.9, R = 0.9
RMSE = 3.0, R = 0.9
POCS05, Pacific Ocean (5 S), -5.0N, -159.0E, 10.0m
RMSE = 37.3, R = 1.0
RMSE = 35.5, R = 1.0
RMSE = 4.9, R = 0.6
RMSE = 4.8, R = 0.6
SEY, Mahe Island, -4.7N, 55.5E, 2.0m
RMSE = 32.4, R = 1.0
RMSE = 32.7, R = 1.0
RMSE = 6.1, R = 0.5
RMSE = 6.1, R = 0.6
POCN00, Pacific Ocean (0 N), 0.0N, -155.0E, 10.0m
RMSE = 38.1, R = 1.0
RMSE = 36.7, R = 1.0
RMSE = 5.7, R = 0.7
RMSE = 5.5, R = 0.7
CH4 (ppb)
Growth rate (ppb/yr)

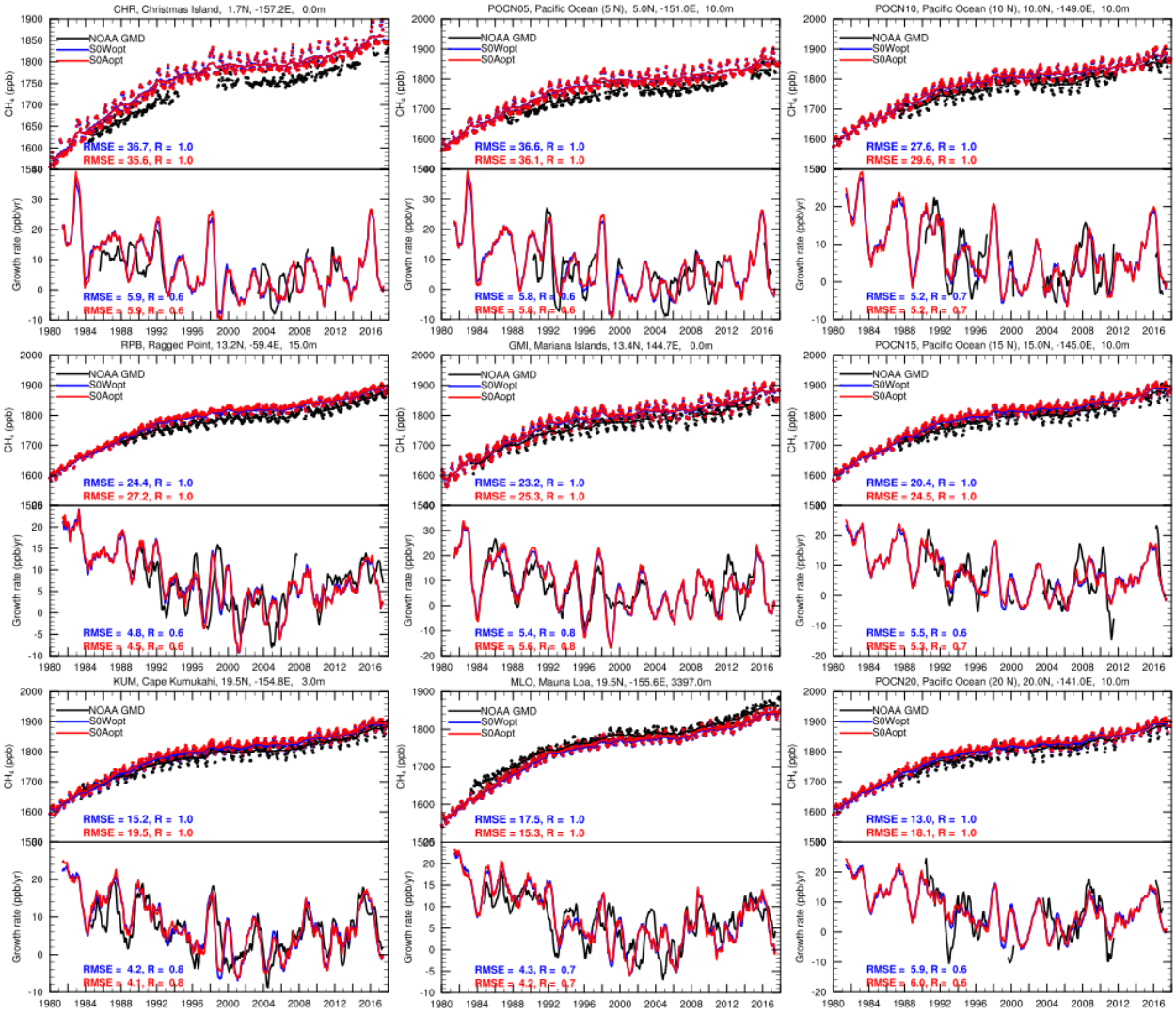
CHR, Christmas Island, 1.7N, -157.2E, 0.0m
NOAA GMD
S0Wopt
S0Aopt
RMSE = 36.7, R = 1.0
RMSE = 35.6, R = 1.0
RMSE = 5.9, R = 0.6
RMSE = 5.9, R = 0.6
POCN05, Pacific Ocean (5 N), 5.0N, -151.0E, 10.0m
RMSE = 36.6, R = 1.0
RMSE = 36.1, R = 1.0
RMSE = 5.8, R = 0.6
RMSE = 5.9, R = 0.6
POCN10, Pacific Ocean (10 N), 10.0N, -149.0E, 10.0m
RMSE = 27.6, R = 1.0
RMSE = 29.6, R = 1.0
RMSE = 5.2, R = 0.7
RMSE = 5.2, R = 0.7
RPB, Ragged Point, 13.2N, -59.4E, 15.0m
RMSE = 24.4, R = 1.0
RMSE = 27.2, R = 1.0
RMSE = 4.8, R = 0.6
RMSE = 4.5, R = 0.6
GMI, Mariana Islands, 13.4N, 144.7E, 0.0m
RMSE = 23.2, R = 1.0
RMSE = 25.3, R = 1.0
RMSE = 5.4, R = 0.8
RMSE = 5.6, R = 0.8
POCN15, Pacific Ocean (15 N), 15.0N, -145.0E, 10.0m
RMSE = 20.4, R = 1.0
RMSE = 24.5, R = 1.0
RMSE = 5.5, R = 0.6
RMSE = 5.3, R = 0.7
KUM, Cape Kumukahi, 19.5N, -154.8E, 3.0m
RMSE = 15.2, R = 1.0
RMSE = 19.5, R = 1.0
RMSE = 4.2, R = 0.8
RMSE = 4.1, R = 0.8
MLO, Mauna Loa, 19.5N, -155.6E, 3397.0m
RMSE = 17.5, R = 1.0
RMSE = 15.3, R = 1.0
RMSE = 4.3, R = 0.7
RMSE = 4.2, R = 0.7
POCN20, Pacific Ocean (20 N), 20.0N, -141.0E, 10.0m
RMSE = 13.0, R = 1.0
RMSE = 18.1, R = 1.0
RMSE = 5.9, R = 0.6
RMSE = 6.0, R = 0.6
CH4 (ppb)
Growth rate (ppb/yr)

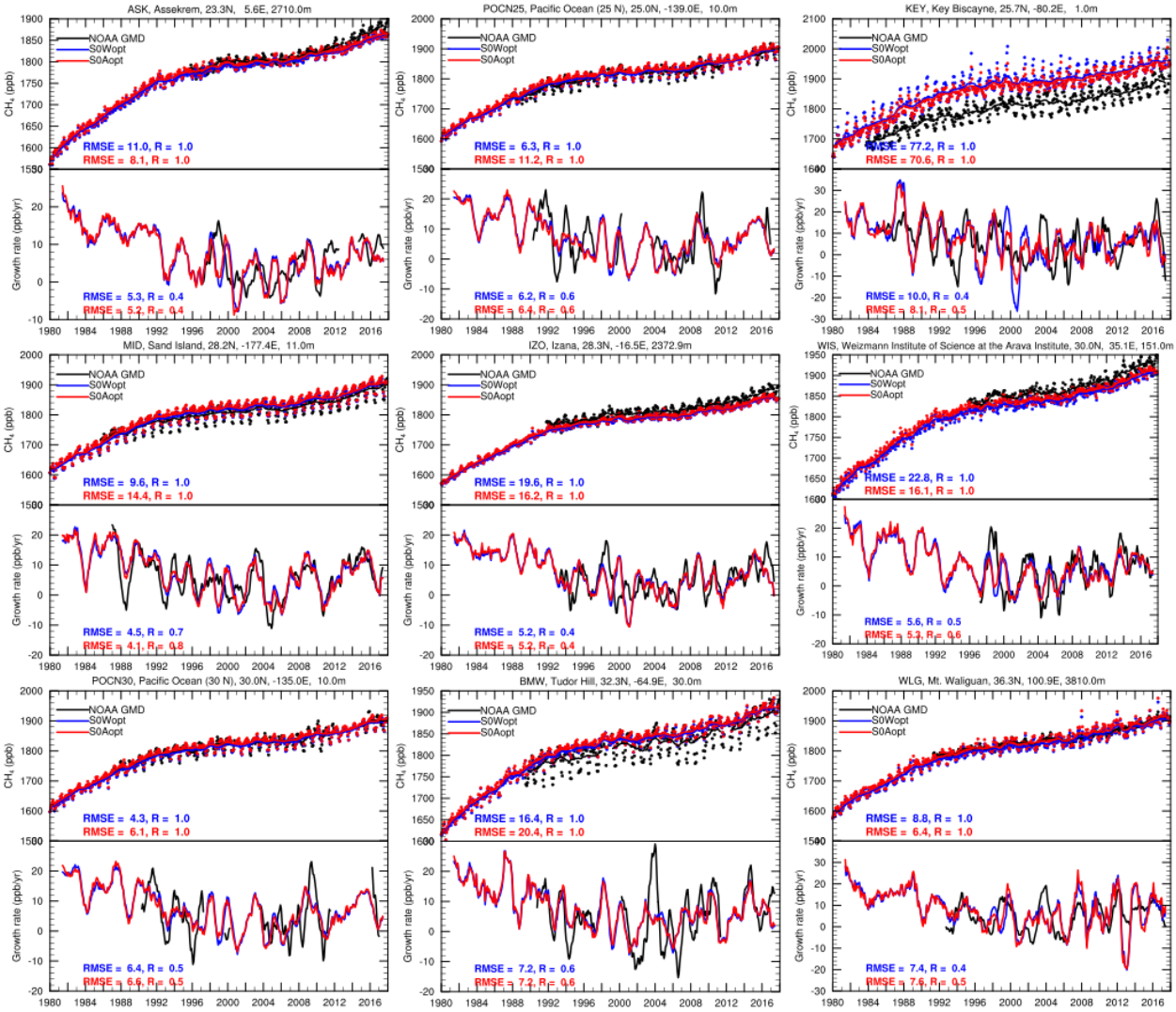
ASK, Assekrem, 23.3N, 5.6E, 2710.0m
POCN25, Pacific Ocean (25 N), 25.0N, -139.0E, 10.0m
KEY, Key Biscayne, 25.7N, -80.2E, 1.0m
MID, Sand Island, 28.2N, -177.4E, 11.0m
IZO, Izana, 28.3N, -16.5E, 2372.9m
WIS, Weizmann Institute of Science at the Arava Institute, 30.0N, 35.1E, 151.0m
POCN30, Pacific Ocean (30 N), 30.0N, -135.0E, 10.0m
BMW, Tudor Hill, 32.3N, -64.9E, 30.0m
WLG, Mt. Waliguan, 36.3N, 100.9E, 3810.0m
NOAA GMD
S0Wopt
S0Aopt
CH4 (ppb)
Growth rate (ppb/yr)

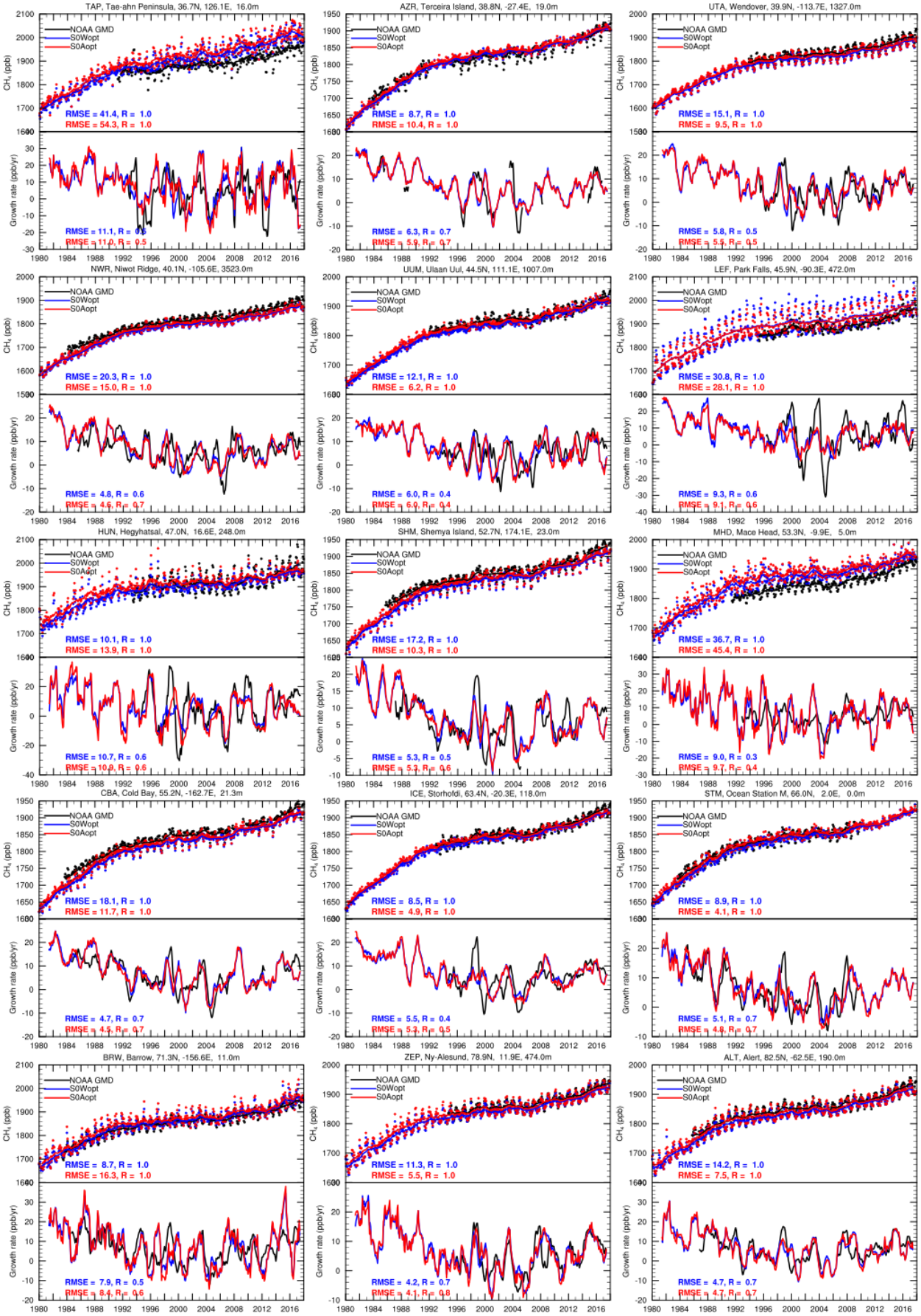

Figure S5. Comparisons of surface CH_4 dry-mole fractions and growth rates to NOAA-GMD observations.

S4. Satellite evaluation

Due to the sparseness of the ground-based observational sites, especially over continental regions, we also evaluate simulated methane against satellite retrievals to reveal information on regional characteristics. Total column-averaged methane DMFs are evaluated against satellite retrievals from the Scanning Imaging Absorption Spectrometer for Atmospheric Chartography (SCIAMACHY) instrument on board the European Space Agency's environmental research satellite ENVISAT (Frankenberg et al., 2011) for January 2003 to April 2012 and the Thermal And Near Infrared Sensor for carbon Observations – Fourier Transform Spectrometer (TANSO-FTS) instrument onboard the Japanese Greenhouse gases Observing SATellite (GOSAT) (Kuze et al., 2016) for April 2009 to December 2016. We compare monthly mean satellite retrievals with simulated monthly mean methane. Retrieval-specific averaging kernels are also applied to simulated monthly mean methane to calculate simulated column-averaged methane DMF.

Unlike the evaluation of global mean surface methane DMF, which is based on observations from a number of sites with well-mixed MBLs, the evaluation of global mean column-averaged methane DMF against satellite retrievals mainly covers continents, considering the impacts from polluted areas and the contributions from the troposphere and the stratosphere. Simulated monthly mean column-averaged methane DMF are compared with satellite retrievals (e.g., SCIAMACHY and GOSAT) in Figure S5. The averaging kernels of SCIAMACHY and GOSAT are individually applied to the model to calculate column-averaged methane abundances. Both simulations are able to capture the monthly variation of methane with R greater than 0.9, but underestimate column-averaged methane, with RMSE of about 21 ppb and 29 ppb when compared to SCIAMACHY and GOSAT retrievals, respectively. The differences in the column-averaged methane abundances between satellite retrievals and model simulations are mostly within 2% except in polar regions where there are large uncertainties in the satellite retrievals. Both simulations are also able to capture the latitudinal distribution of the column-averaged methane DMF with R close to 1.

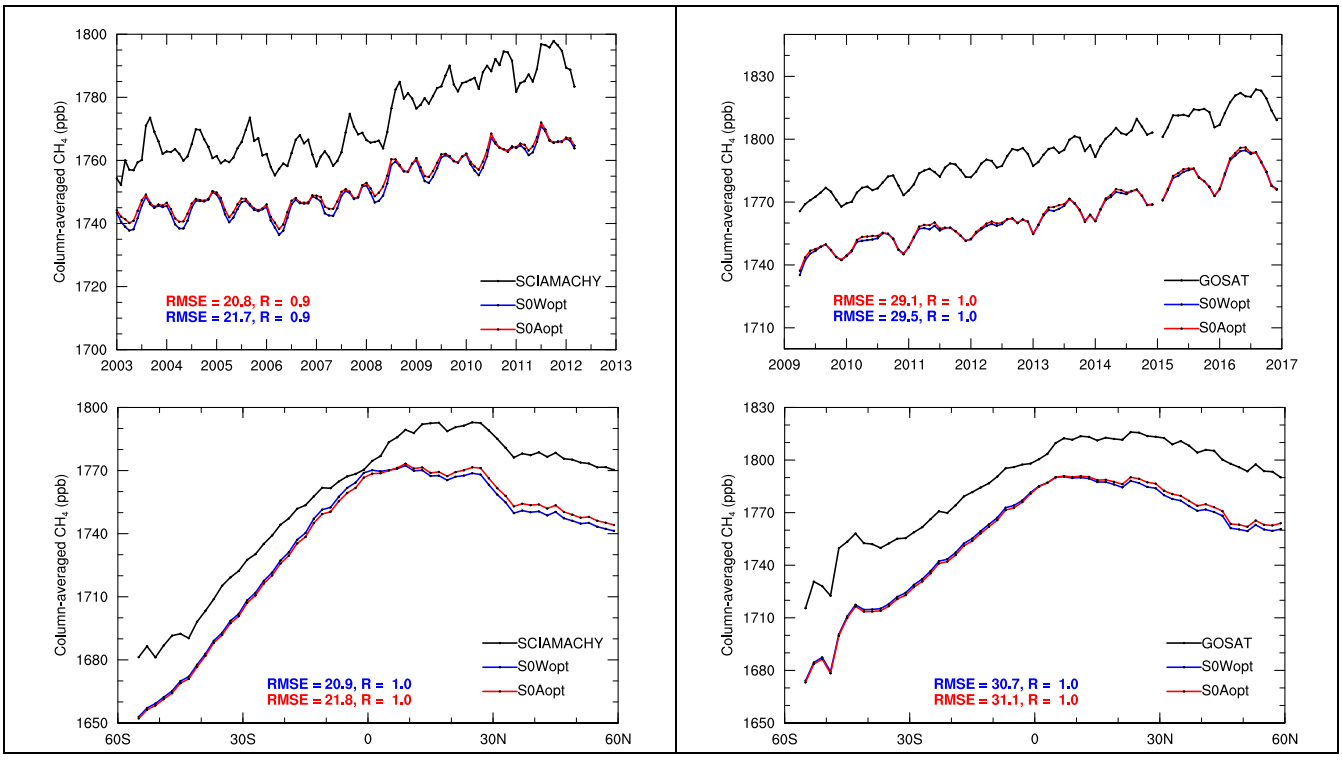

Figure S6. Comparisons of column-averaged methane concentrations with SCIAMACHY (left) and GOSAT (right) satellite retrievals.

S5. Spatial distribution

As described in Section 2.3, the emission optimization is conducted for anthropogenic sectors (i.e., S0Aopt) and wetland sector (i.e., S0Wopt). Although global total methane emissions are the same for S0Aopt and S0Wopt, they have different allocations for anthropogenic and wetland sectors and different spatial distributions as well. Here we analyze the sensitivity of sector optimization on the spatial distribution of simulated methane concentrations. Figure S7 shows the spatial distributions of the simulated methane DMF at surface by S0Aopt and S0Wopt and Figure S8 shows the spatial distributions of the differences in surface methane abundance between S0Aopt and S0Wopt during the four periods (i.e., 1980-1989, 1990-1999, 2000-2006, and 2007-2017). Surface methane is always lower in Aopt than Wopt in the tropics (e.g., 15^{o} S-10^{o} N) during the four periods. This is mainly due to much lower wetland emissions in S0Aopt than in S0Wopt (Figure S9), which dominates total emissions over these regions (e.g., tropical South America and Central Africa). There is not much difference in surface methane over low and high southern latitudes (e.g., 15-90^{o} S) between the two simulations. This agreement is mainly because larger anthropogenic emissions in S0Aopt compensate smaller wetland emissions, producing only small differences in the total emissions, within 0.1 Tg yr^{-1}. Unlike the Southern Hemisphere, surface methane concentrations are in general higher in S0Aopt than S0Wopt in the Northern Hemisphere, especially over the Eastern U.S. and Eurasia, due to much higher anthropogenic emissions in S0Aopt. The lower surface methane values in S0Aopt over northern Canada are due to much lower wetland emissions in S0Aopt.

Figure S10 shows the methane growth rates simulated by Aopt and Wopt during the four time periods. Global mean methane growth rates simulated by Aopt and Wopt are very consistent during the four periods, with growth rates decreasing from 1980s to 1990s, stabilizing during 2000-2006, and increasing after 2007. During the 1980s and 1990s, methane growth rates in both S0Aopt and S0Wopt increase over most of the globe except a decrease over Russia, due to significant decreases in anthropogenic emissions (mainly from the energy sector) in the former Soviet Union, consistent with previous studies (Dlugokencky et al., 2011). During 2000-2006, methane growth rates increase significantly over East Asia in both S0Aopt and S0Wopt while they decrease over tropical South America and Central Africa in S0Wopt but not in Aopt. This is mainly due to decreases in wetland emissions in the S0Wopt case, while wetland emissions are constant for each year in Aopt case. After 2007, both Aopt and Wopt suggest large increases in methane growth rates over East Asia (mainly due to increases in anthropogenic emissions) by up to ~38 ppb yr^{-1} with smaller increases elsewhere (< 7 ppb yr^{-1}) while noticeable increases over the Arctic (> 7 ppb yr^{-1}). The relatively large methane growth over the Arctic is mainly due to increases in anthropogenic methane from lower latitudes.

As discussed in Sections 3.1 and 3.2, the similarity in S0Aopt and S0Wopt simulation results suggests that for 3-dimensional chemistry transport models, reasonable estimates of total global methane emissions are critical for global methane predictions, despite the uncertainties in the spatial distribution of the emissions and in the estimates of individual sources, which are more important for regional methane predictions. At the same time, accurate estimates of individual sources are necessary to attribute the methane trend and variability into individual sources.

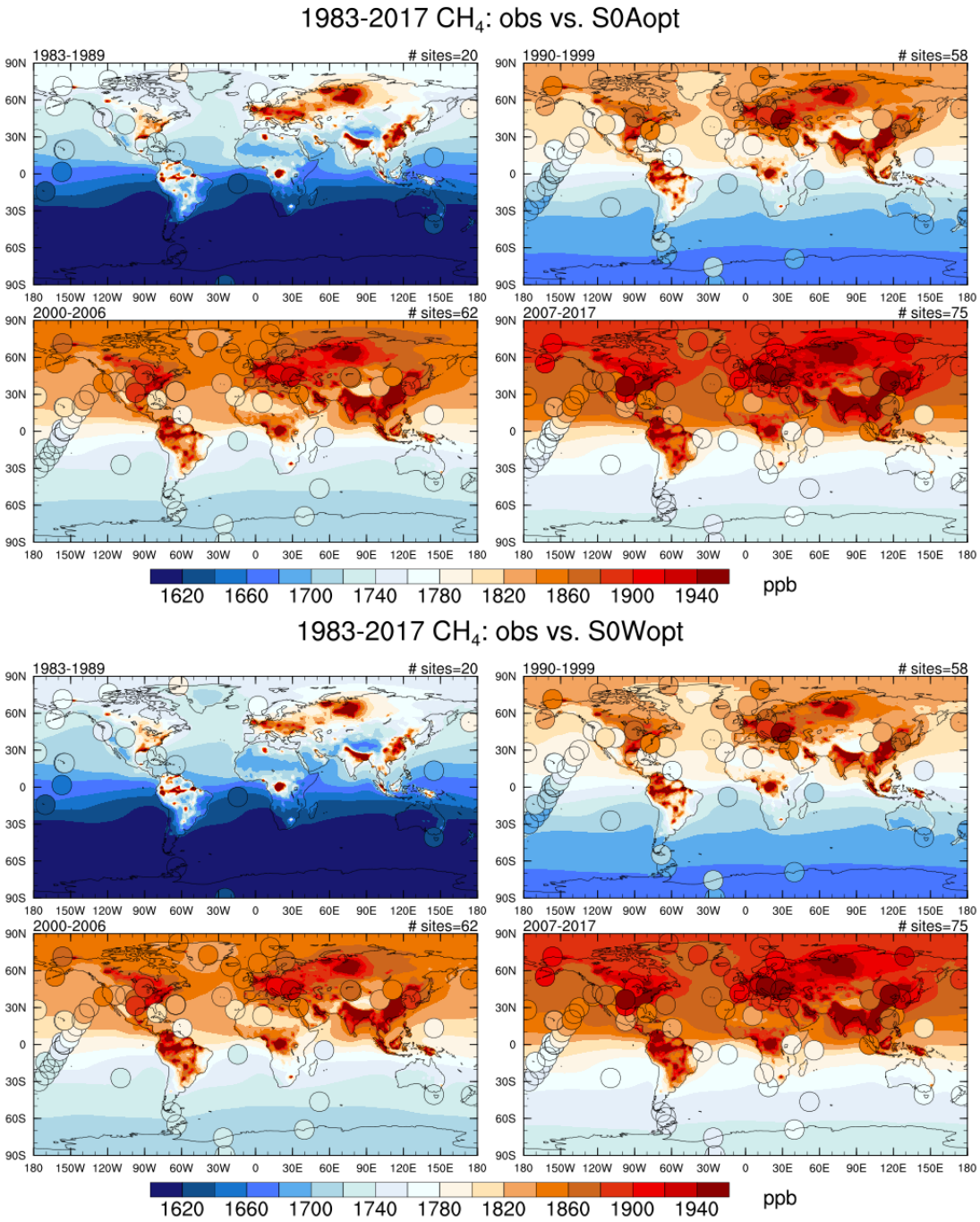

Figure S7. Surface CH_4 dry-air mole fractions by S0Aopt and S0Wopt overlaid with NOAA-GMD surface observations for the periods of 1980-1989, 1990-1999, 2000-2006, and 2007-2017. The circles represent observations at individual sites.

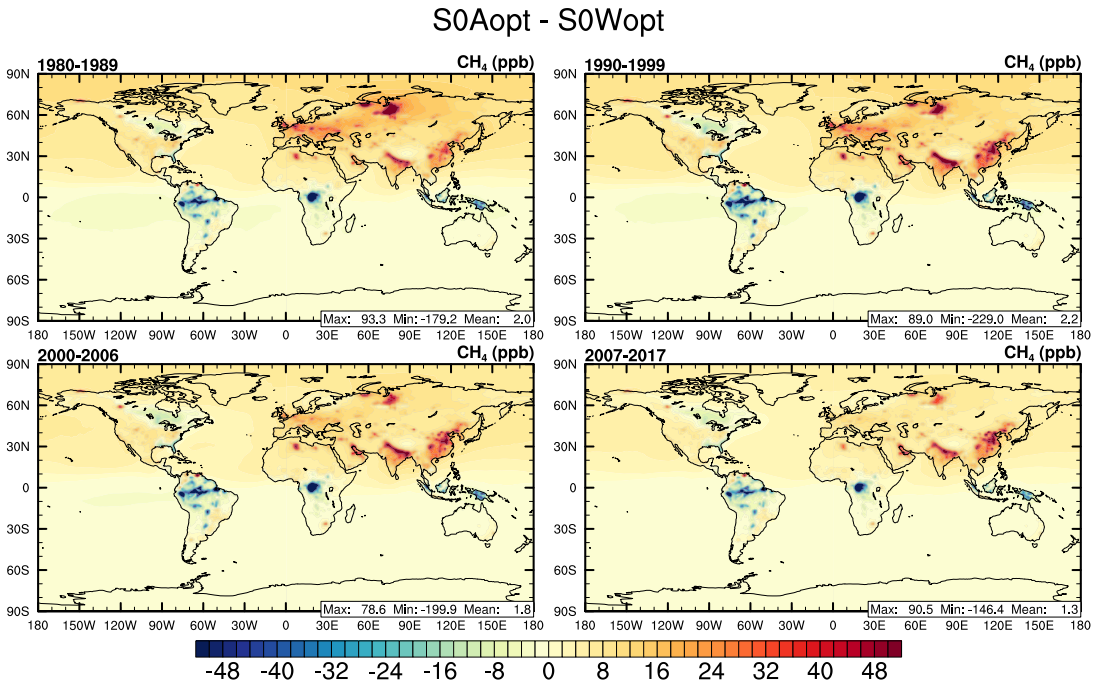

Figure S8. Absolute difference in surface CH_4 predictions between S0Aopt and S0Wopt for the periods of 1980-1989, 1990-1999, 2000-2006, and 2007-2017.

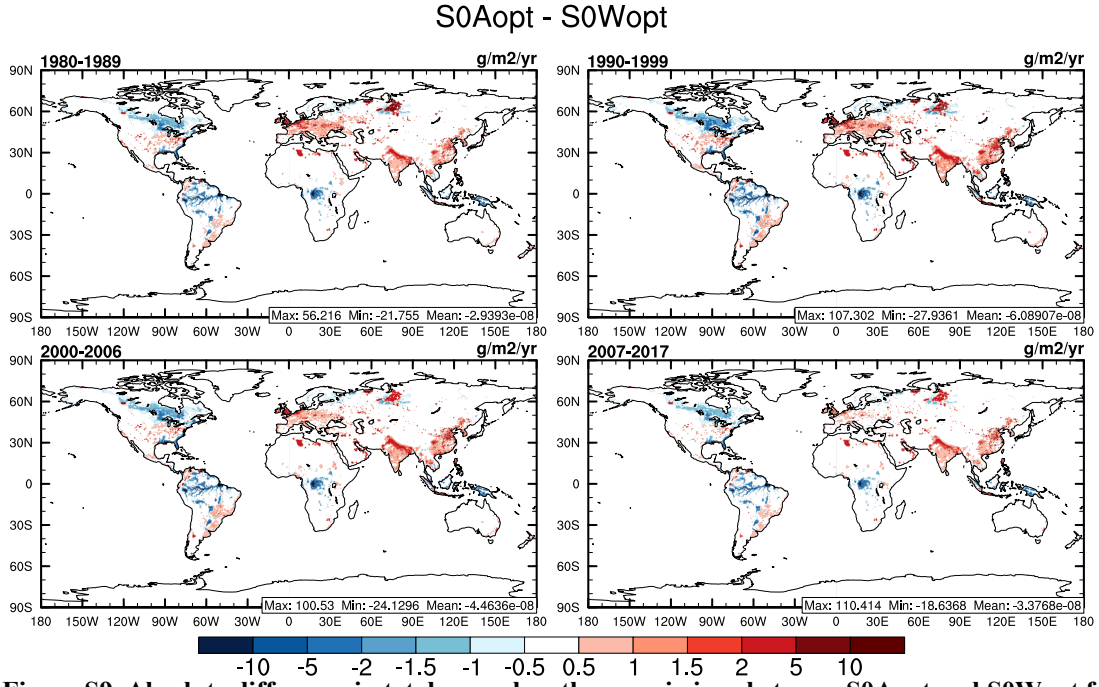

Figure S9. Absolute difference in total annual methane emissions between S0Aopt and S0Wopt for the periods of 1980-1989, 1990-1999, 2000-2006, and 2007-2017.

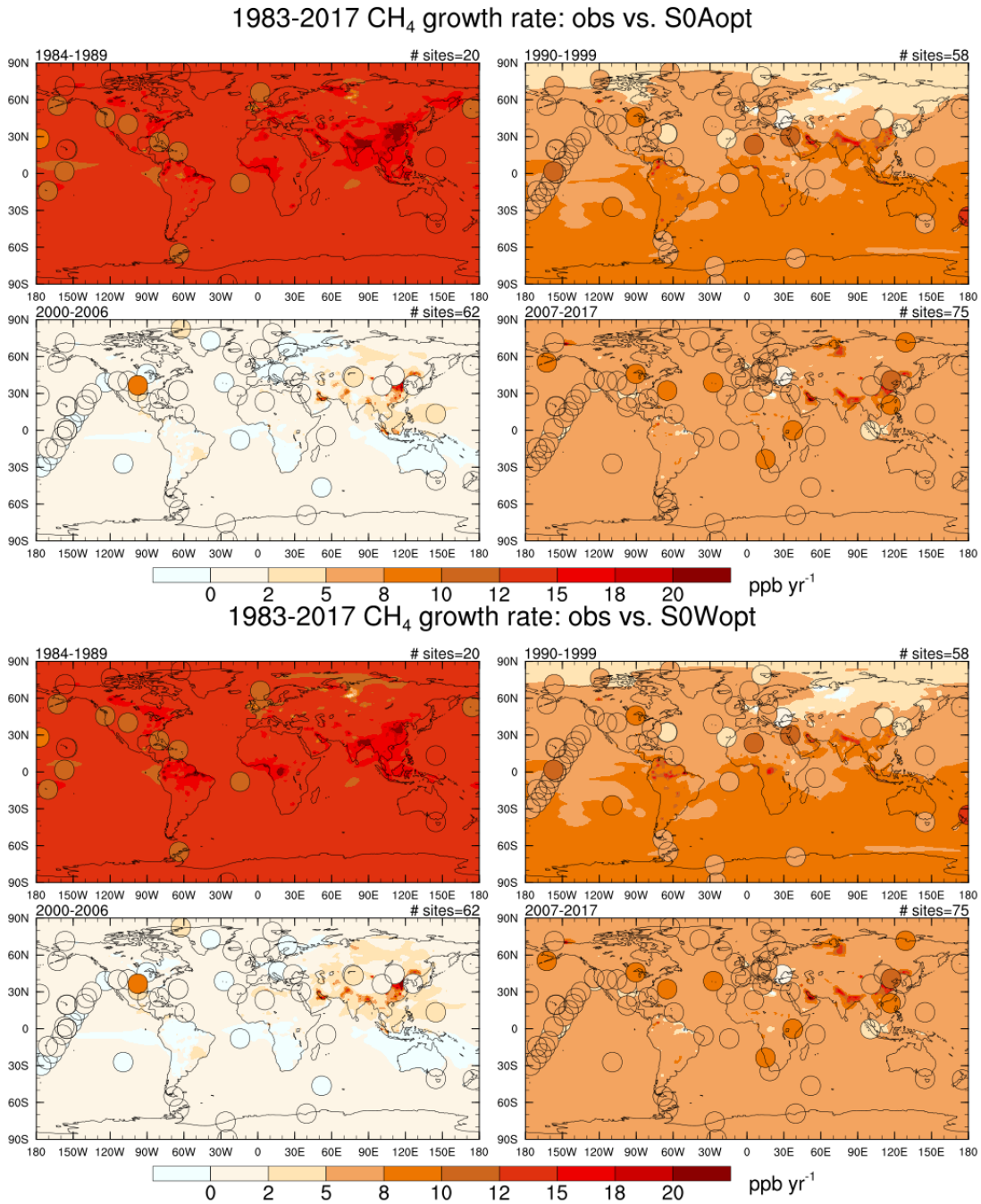

Figure S10. Spatial distribution of surface methane growth (ppb/yr) by S0Aopt (upper panel) and S0Wopt (lower panel) overlaid with NOAA-GMD surface observations for the periods of 1980-1989, 1990-1999, 2000-2006, and 2007-2017. The circles represent observations at individual sites.

References:

Bloom, A. A., Bowman, K. W., Lee, M., Turner, A. J., Schroeder, R., Worden, J. R., Weidner, R., McDonald, K. C., and Jacob, D. J.: A global wetland methane emissions and uncertainty dataset for atmospheric chemical transport models (WetCHARTs version 1.0), Geosci. Model Dev., 10, 2141-2156, https://doi.org/10.5194/gmd-10-2141-2017, 2017.

Dlugokencky, E. J., Nisbet, E. G., Fisher, R., and Lowry, D.: Global atmospheric methane: budget, changes and dangers, Philos. T. R. Soc. A, 369, 2058–2072, 2011.

Frankenberg, C., Fisher, J. B., Worden, J., Badgley, G., Saatchi, S. S., Lee, J.-E., Toon, G. C., Butz, A., Jung, M., Kuze, A., and Yokota, T.: New global observations of the terrestrial carbon cycle from GOSAT: patterns of plant fluorescence with gross primary productivity, Geophys. Res. Lett., 38, 1–6, doi:10.1029/2011GL048738, 2011.

Kuze, A., Suto, H., Shiomi, K., Kawakami, S., Tanaka, M., Ueda, Y., Deguchi, A., Yoshida, J., Yamamoto, Y., Kataoka, F., Taylor, T. E., and Buijs, H. L.: Update on GOSAT TANSO-FTS performance, operations, and data products after more than 6 years in space, Atmos. Meas. Tech., 9, 2445-2461, doi:10.5194/amt-9- 2445-2016, 2016.

Tans, P. P., Conway, T. J., and Nakazawa, T.: Latitudinal distribution of the sources and sinks of atmospheric carbon dioxide derived from surface observations and an atmospheric transport model, J. Geophys. Res., 94, 5151–5172, doi:10.1029/JD094iD04p05151, 1989.

Thoning, K. W.: Curve Fitting Methods Applied to Time Series in NOAA/ESRL/GMD, path: https://www.esrl.noaa.gov/gmd/ccgg/mbl/crvfit/crvfit.html, 2019.

Thoning, K.W., Tans, P. P., and Komhyr, W. D.: Atmospheric carbon dioxide at Mauna Loa Observatory, 2. Analysis of the NOAA/GMCC data, 1974-1985, J. Geophys. Res., 94, 8549-8565, 1989.